Surface warming by the solar cycle as revealed by the composite mean difference projection

Charles D. Camp[1] and Ka Kit Tung[1]

Received 29 March 2007; revised 15 May 2007; accepted 14 June 2007; published 18 July 2007.

[1] By projecting surface temperature data (1959–2004) onto the spatial structure obtained objectively from the composite mean difference between solar max and solar min years, we obtain a global warming signal of almost 0.2°K attributable to the 11-year solar cycle. The statistical significance of such a globally coherent solar response at the surface is established for the first time. **Citation:** Camp, C. D., and K. K. Tung (2007), Surface warming by the solar cycle as revealed by the composite mean difference projection, *Geophys. Res. Lett.*, *34*, L14703, doi:10.1029/2007GL030207.

1. Introduction

[2] Because of the variations of sunspots and faculae on the sun's surface, the total solar irradiance (TSI), also called the solar constant, varies on a roughly 11-year cycle by about 0.07%, which has been measured by orbiting satellites since 1978 [*Lean*, 1987, 1991; *Wilson et al.*, 1981]. The change in the solar constant amounts to about 0.90 Wm^{-2} for the last three cycles. There have been thousands of reports over two hundred years of regional climate responses to the 11-year variations of solar radiation, ranging from cycles of Nile River flows, African droughts, to temperature measurements at various selected stations, but a coherent global signal at the surface has not yet been established statistically [*Hoyt and Schatten*, 1997; *Pittock*, 1978]. Since the forcing is global, theoretically one should expect a global-scale response. When globally and annually averaged and detrended, but otherwise unprocessed, the surface air temperature since 1959 (when modern rawinsonde network was established) is seen in Figure 1 to have an interannual variation of about 0.2°K, somewhat positively correlated with the solar cycle, although the signal also contains a higher frequency (of 3–5 year period) variation of comparable magnitude, possibly due to El Niño-Southern Oscillation (ENSO). What is surprising is that a solar-cycle signal is already apparent in this "raw" data. An isospectral Monte-Carlo test shows that the correlation coefficient, $\rho = 0.47$, between the global temperature and the TSI is statistically significant at 98.4% confidence level. This is obtained without any filtering of the global mean signal, and gives confidence that the solar signal is not an artifact of our filtering to be presented below. The "solar cycle signal" obtained by regressing the global mean temperature onto the TSI time series yields the regression coefficient of $\kappa = 0.18 \pm 0.10$°K per Wm^{-2} of solar constant variation, suggesting a mean global warming of ~0.16°K from solar min to solar max. Next we will use a spatial filter to obtain a cleaner solar-cycle signal.

2. Composite Mean Difference (CMD) Projection

2.1. Spatial Pattern

[3] One powerful approach is to take advantage of the spatial characteristics of the solar-cycle response. One intuitive way to obtain the spatial pattern is to use the difference of the solar-max composite and the solar-min composite. Figure 2a shows the meridional pattern of the composite-mean difference for the zonal-mean, annual-mean air temperature at the surface using the global dataset of NCEP [*Kalnay et al.*, 1996], linearly detrended to remove the secular global-warming signal. Composite differences have often been used to deduce the pattern of solar-cycle response [*Labitzke et al.*, 2002]. However, the difficulty lies in verifying the statistical significance of the pattern generated by this method; since even with an arbitrary partition into any two groups, there is always a difference pattern. Here we employ an additional step of projecting our original detrended data onto this spatial pattern, in effect using it as a spatial filter, and generating a *time* series, shown in Figure 2c. It is seen that this procedure effectively filters out the higher-frequency variability, since presumably the latter has a different spatial pattern. The filtered temperature time series now has a much higher correlation with the solar TSI index, with a higher correlation coefficient of $\rho = 0.64$ but the same (mean) regression amplitude of $\kappa = 0.18 \pm 0.08$°K per Wm^{-2}, although with a 20% smaller error bar.

2.2. Statistical Significance

[4] We can now test the statistical significance of our "solar-cycle signal" by asking what the likelihood is that the observed correlation, $\rho = 0.64$, could be obtained randomly. We address this question (the answer: 0.2%) using a bootstrap Monte-Carlo test, which randomly assigns years, with replacement, to the two groups; the result is shown in Figure 2b. It establishes that the observed correlation of the spatially filtered surface temperature with the 11-year solar cycle is statistically significant at 99.8% confidence level. This is the first time a coherent global pattern of response to solar cycles has been shown to be statistically significant (see the critique of *Coughlin and Tung* [2006] on the spatial pattern of *Gleisner and Thejll* [2003] obtained through correlation coefficients).

[5] Early estimates of the solar-cycle response were obtained using *model-generated* "optimal space-time filter"[*Stevens and North*, 1996], whose pattern is small over the poles as compared to the tropics. This, and a shorter time record, may be the reason for the smaller global-mean surface temperature obtained, about 0.06 K.

[1]Department of Applied Mathematics, University of Washington, Seattle, Washington, USA.

0094-8276/07/2007GL030207$05.00

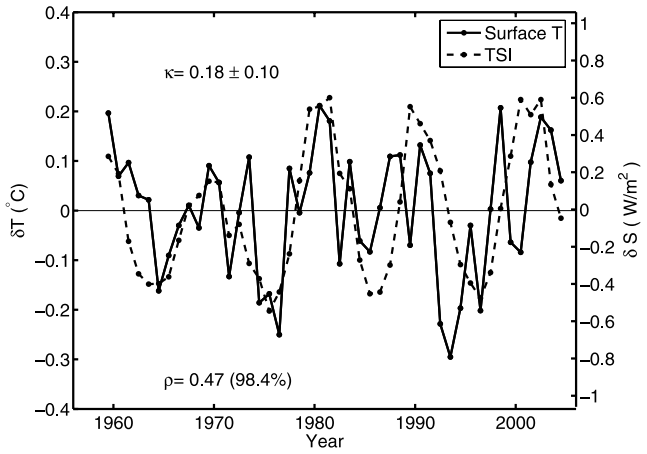

Figure 1. Annual-mean, global-mean NCEP surface air temperature (1959–2004), solid line, with scale on the left axis. The dashed line shows the annual-mean TSI time series [*Lean et al.*, 1995], updated and provided to us by Dr. J. Lean, with scale on the right axis. κ is the regression of global-mean temperature response in °K per each Wm^{-2} variation of the solar constant. ρ is the correlation coefficient between the global temperature and the TSI. An isospectral Monte-Carlo test, in which the spectral phase of the temperature (or the TSI) time series is randomized while preserving the spectral amplitude to generate 3,000 synthetic time series, shows that this positive value of ρ is not likely to occur by chance.

Other previously used methods, such as multiple regression methods and composite differences, have not been able to establish a statistically significant coherent global pattern. In the multiple regression method, the time series at each spatial location is analyzed independently of the time series from other locations. Although a spatial pattern of the solar-cycle response can be reconstructed afterwards by piecing together the regression coefficients for the solar-cycle index from each location, it turns out that over most of the globe, with the exception of two strips near the midlatitudes, the signal falls below statistical significance [see *Haigh*, 2003]. In the work of *Labitzke et al.* [2002], the composite-mean difference obtained by them was not used in the statistical test of the correlation coefficient. The latter was obtained separately by correlating the original time series at each location with the solar-cycle index. These previous methods do not take advantage of the spatial information of the response. We have obtained higher statistical significance by first filtering the time series through this spatial filter. One variability that our spatial filter may not remove is the volcanic-aerosol cooling, which probably has a similar global distribution. It however can be removed in the temporal domain. Volcanic eruptions, particularly El Chichón in March 1982 and Pinatubo in June 1991, coincidentally occurring during solar maxes, may contaminate the 11-year signal. The expected cooling in the troposphere for the transient aerosol events however lasted only temporarily, for about two to three years. Since our method does not

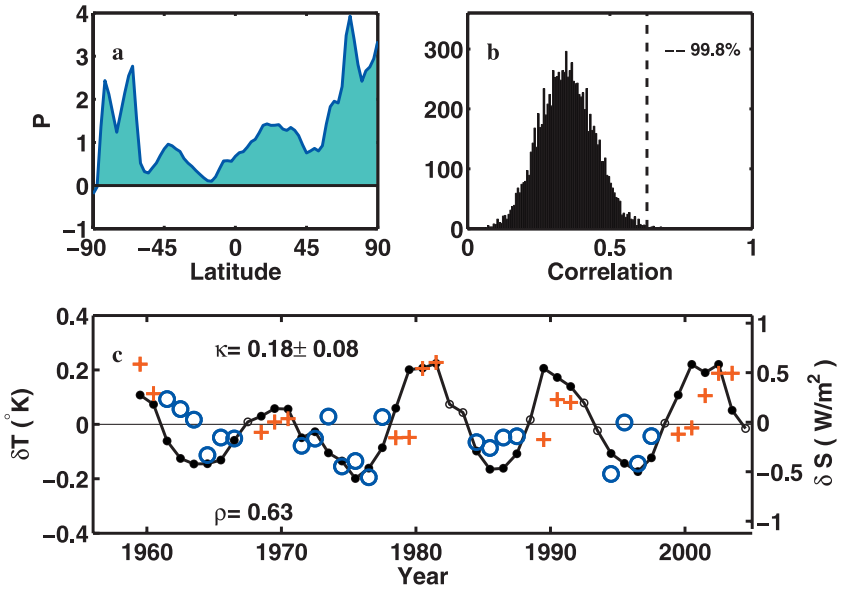

Figure 2. Surface temperature from NCEP 1959-2004 in 2.5° latitude resolution. (a) The latitudinal pattern of the zonal-mean annual-mean surface temperature in the years in the solar-max group (when TSI is 0.06 Wm^{-2} above the mean) minus the years in the solar-min group (when TSI is 0.06 below the mean), normalized so that its global mean is one. (b) Monte-Carlo test of the correlation coefficient ρ using 10,000 synthetic time series generated using random assignments of the solar-max and solar- min groups while preserving the same number of years in each group, and projection onto their composite-mean difference. Plotted are the number of occurrences of the synthetic time series vs their correlation coefficients. The observed value of $\rho = 0.64$ is indicated by a vertical line. It is found to occur by chance only 0.2% of the time. (c) Projection of the original detrended time series onto the spatial pattern, yielding the time-dependent index. The red pluses are temperatures in the solar-max group and the blue circles are in the solar-min group. The black line shows the annual mean TSI time series with scale on the right axis. The small solid circles indicate the years used in the analysis, while the hollow small circles indicate the years dropped. These are the years of the volcanoes discussed in the text.

require a continuous time series, the volcano aerosol years can be excluded from the time series. This has been done in Figure 2, where the years 1982 and 1983 (after El Chichón), and 1992 and 1993 (after Pinatubo) are excluded. The greenhouse warming signal is removed to the extent possible by the linear trend. However, the linear trend may be sensitive to the end point and unfortunately 2005 is a very unusual year (one of the warmest on record). To minimize this end-point error, only 1959–2004 were used in the analysis. To include 2005, a nonlinear trend may need to be used. The single linear trend used here does not work well for the ERA-40 data, which has different signed linear trends before and after 1979.

3. Polar Warming

[6] The surface pattern in Figure 2 shows clearly the polar amplification of warming, predicted also by models for the global-warming problem, with largest warming in the Arctic (3 times that of the global mean), followed by that of the Antarctic (2 times). Since the tropical atmosphere is more opaque, a warmed surface cannot re-radiate all the energy it receives back to space unless it is much warmer. The excess radiative energy must be transported by dynamic heat fluxes to the high latitudes, resulting in polar warming [*Cai*, 2005]. This occurs rather quickly, in 5 years or less, and probably involves mostly the atmosphere and the upper oceans, as *White et al.* [1997] showed that the solar-cycle response does not penetrate deep enough in the ocean to engage the deep water. Low warming occurs over the latitudes of the Southern ocean and over the Southern tropics. These general features are similar to those predicted for global warming [*Manabe and Stouffer*, 1980].

[7] We have repeated the calculation using only the tropical data and obtained κ and ρ very similar to those for the global mean temperature signal in Figure 1. Higher κ is found for each of extratropics, but with higher error bars, implying higher variability in the extratropical signals. Although all three regions are individually significant under a Monte-Carlo test, higher ρ and smaller error bars are found only when all three regions are combined to form a coherent spatial pattern.

4. Amplitude of the Global Warming

[8] Our work establishes that the surface-temperature response is correlated with the solar-cycle forcing at over 95% confidence level. For comparison, a similar relationship between response and forcing has not been statistically established for the greenhouse global-warming problem. Our result shows a global-mean warming of almost 0.2°K at the surface from solar min to solar max. More precisely, we fit $\delta T = \kappa \delta S$ to all 4.5 solar cycles, where $\delta S(t)$ is the TSI variability time series, and find $\kappa = 0.18 \pm 0.08$°K/(Wm^{-2}) at the surface. The error bars define a 95% confidence interval and are approximately equal to ±2 standard deviations (σ). This value of κ is about 50–70% higher than the regression coefficients of temperature against irradiance variability previously deduced [*Douglass and Clader*, 2002; *Lean*, 2005; *Scafetta and West*, 2005], of ~0.1°K global- mean surface warming attributable to the solar cycles. This result is consistent with the earlier finding of *Coughlin and Tung* [2004] using a completely different method in the time domain, who also found the zonal-mean warming to be positively correlated with the solar-cycle index over most of the troposphere. Our higher response level is also consistent with some other recent reports from observation [*Haigh*, 2003; *Labitzke et al.*, 2002; *van Loon et al.*, 2004].

[9] A more novel optimization method, the Linear Discriminant Analysis, can be used to obtain a better bound with half the magnitude of the error bars. The LDA method finds the optimal spatial structure that best separates the solar-max group from the solar-min group [*Schneider and Held*, 2001; *Camp and Tung*, 2007a, 2007b]. This result is reported in a forthcoming paper. The present CMD Projection method has the advantage of being more intuitive and the result easier for others to reproduce.

5. Detailed Spatial Pattern

[10] Having established the existence of a global-scale solar-cycle response, we next examine in more detail the surface warming pattern over the globe. We repeat the CMD Projection analysis on the gridded NCEP surface air-temperature data at a latitude-longitude resolution of 5° × 5°. Consistent with the zonal mean pattern shown in Figure 2, the largest warming in Figure 3 occurs over the two polar regions. Warming of about 0.7°K occurs near seasonal sea-ice edges around the Antarctic continent and the Arctic Ocean, strongly suggestive of positive ice-albedo feedback as a mechanism for the polar amplification of the radiative forcing. Although the whole of the western Arctic is warm, largest warming occurs around the "Northwest Passage" (the Canadian Archipelago, Beaufort Sea, the coast of northern Alaska and the Chukchi Sea between Alaska and Siberia). The warm pattern is quite similar to the observed recent trend [*Moritz et al.*, 2002], and may suggest a common mechanism to the extent that the data in these locations can be trusted. In the midlatitudes, there is more warming over the continents than over the oceans. Most of Europe is warmed by 0.3°K, and eastern Canada by 0.4°K, while western U.S. sees a smaller warming of 0.2°K. Over the tropics, not much warming occurs whether it is over land or over ocean. The warming over the tropics instead occurs higher up, at 200 hPa (not shown, at only 90% confidence level because of the quality of the upper air data prior to 1979), which is where the latent heat due to vertical convection is deposited. *Cai* [2005] discusses how, in the greenhouse warming problem, the vertical transport of surface heating in a moist atmosphere leads to an increase in poleward heat transport despite the weakening of the surface-temperature gradient due to polar amplification of warming. In the equatorial Pacific, there is a weak anti-El Niño signal of cooling over the eastern Pacific off the coast of Peru and warming over the west Pacific near Papua New Guinea. This change in climatology over decadal scales is retained while the difference between El Niño and La Niña is filtered out by our method. This non-intuitive pattern may be explainable using the ocean "thermostat" mechanism of *Clements et al.* [1996], whereby a basin-wide uniform heating results in a warmer western Pacific, but does not heat the eastern Pacific, which is controlled by the cold deep water below the shallow thermocline there. The increased

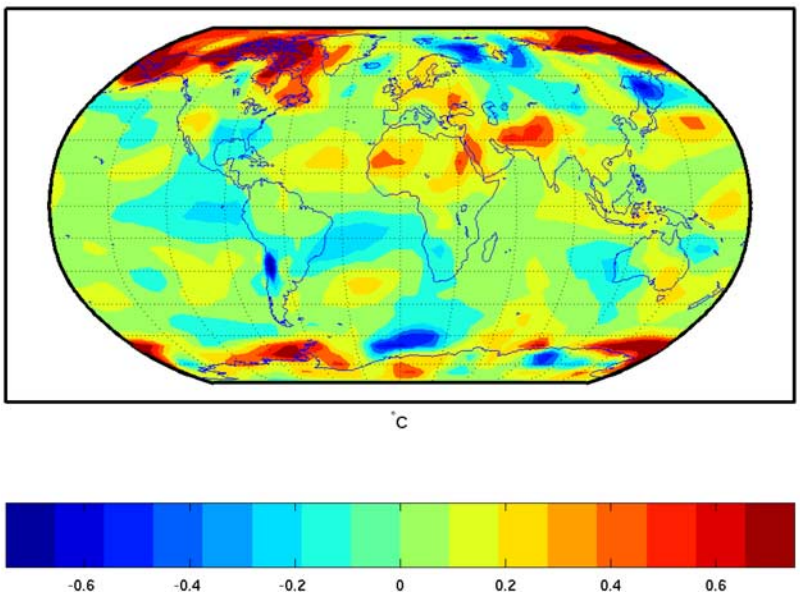

Figure 3. The global-surface pattern of temperature obtained by composite-mean difference (solar-max group minus solar-min group) in $5° \times 5°$ resolution. Shown in color is the temperature difference in °K between ± one standard deviation from the mean. The actual peak-to-peak difference between the solar max and solar min is larger, but not as robust as the standard-deviation difference. A measure of the peak-to-peak difference can be obtained by multiplying the values shown by a factor of $\pi/2$. Monte-Carlo test shows that this global pattern is statistically significant above the 95% confidence level, although the test does not apply to individual locations.

east-west temperature gradient drives a stronger Walker cell during solar max, creating a La Niña-like ocean pattern. This pattern has been reproduced in the Cane-Zebiac model and appears to be consistent with paleo records during the Medieval Maximum of solar activity, and with an opposite pattern during the Maunder Minimum or the colder climate following a major volcanic eruption [*Mann et al.*, 2005]. Recently, *van Loon et al.* [2007] found a similar cold pattern in the equatorial Pacific by compositing 11 peak solar years versus the climatology. They also attributed the pattern to the strengthened Walker circulation. It should be noted here that the amplitude of our equatorial Pacific pattern is small compared with that of ENSO and could change if the period under consideration is changed (with more or less El Niño occurrences).

6. Conclusion

[11] We propose that spatial information be used to filter the surface-temperature data to obtain a cleaner solar-cycle response. At the global scales, an objectively determined spatial filter can be constructed using the composite difference between the solar-max years and the solar-min years. This filter effectively removes the shorter interannual variations, such as from ENSO. We obtained a globally averaged warming of almost 0.2°K during solar max as compared to solar min, somewhat larger than previously reported. More importantly, we have established that the global-temperature response to the solar cycle is statistically significant at over 95% confidence level. The spatial pattern of the warming is also of interest, and shows the polar amplification expected also for the greenhouse-warming problem. The method used here, the CMD Projection, is one of two methods we have tried that take advantage of the spatial information, the other method being the LDA method. Although not as optimal as the LDA method, the CMD Projection possesses most of the advantages of the former while being much simpler to understand and implement. As it turns out, the spatial patterns deduced by the two different methods are very close to each other. However, the LDA method yields a more accurate estimate of the solar-cycle response in the sense that its error bar is only half as large.

[12] We will argue in a separate paper that the observed warming is caused mostly by the radiative heating (TSI minus the 15% absorbed by ozone in the stratosphere), when taking into account the positive climate feedbacks (a factor of 2–3) also expected for the greenhouse warming problem.

[13] **Acknowledgments.** The research is supported by grant ATM-3 32364 from National Science Foundation, Climate Dynamics Program. We thank Judith Lean for providing us with her reconstructed TSI and UV time series.

References

Cai, M. (2005), Dynamical amplification of polar warming, *Geophys. Res. Lett.*, *32*, L22710, doi:10.1029/2005GL024481.

Camp, C. D., and K. K. Tung (2007a), The influence of the solar cycle and QBO on the late winter stratospheric polar vortex, *J. Atmos. Sci.*, *64*, 1267–1283.

Camp, C. D., and K.-K. Tung (2007b), Stratospheric polar warming by ENSO in winter: A statistical study, *Geophys. Res. Lett.*, *34*, L04809, doi:10.1029/2006GL028521.

Clements, A. C., et al. (1996), An ocean dynamical thermostat, *J. Clim.*, *9*, 2190–2196.

Coughlin, K., and K. K. Tung (2004), Eleven-year solar cycle signal throughout the lower atmosphere, *J. Geophys. Res.*, *109*, D21105, doi:10.1029/2004JD004873.

Coughlin, K. T., and K. K. Tung (2006), Misleading patterns in correlation maps, *J. Geophys. Res.*, *111*, D24102, doi:10.1029/2006JD007452.

Douglass, D. H., and B. D. Clader (2002), Climate sensitivity of the Earth to solar irradiance, *Geophys. Res. Lett.*, *29*(16), 1786, doi:10.1029/2002GL015345.

Gleisner, H., and P. Thejll (2003), Patterns of tropospheric response to solar variability, *Geophys. Res. Lett.*, *30*(13), 1711, doi:10.1029/2003GL017129.

Haigh, J. D. (2003), The effects of solar variability on the Earth's climate, *Philos. Trans. R. Soc. London, Ser. A*, *361*, 95–111.

Hoyt, D. V., and K. H. Schatten (1997), *The Role of the Sun in Climate Change*, 279 pp., Oxford Univ. Press, New York.

Kalnay, E., et al. (1996), The NCEP/NCAR 40-year reanalysis project, *Bull. Am. Meteorol. Soc.*, *77*, 437–471.

Labitzke, K., et al. (2002), The global signal of the 11-year solar cycle in the stratosphere: Observations and models, *J. Atmos. Sol. Terr. Phys.*, *64*, 203–210.

Lean, J. (1987), Solar ultraviolet irradiance variations: A review, *J. Geophys. Res.*, *92*, 839–868.

Lean, J. (1991), Variations in the Sun's radiative output, *Rev. Geophys.*, *29*, 505–535.

Lean, J. (2005), Living with a variable Sun, *Phys. Today*, *58*, 32–38.

Lean, J., J. Beer, and R. Bradley (1995), Reconstruction of solar irradiance since 1610: Implications for climate change, *Geophys. Res. Lett.*, *22*(23), 3195–3198.

Manabe, S., and R. J. Stouffer (1980), Senstivity of a global climate model to an increase of CO_2 concentration in the atmosphere, *J. Geophys. Res.*, *85*, 5529–5554.

Mann, M. E., et al. (2005), Volcanic and solar forcing of the tropical Pacific over the past 1000 years, *J. Clim.*, *18*, 447–456.

Moritz, R. E., et al. (2002), Dynamics of recent climate change in the Arctic, *Science*, *297*, 1497–1502.

Pittock, A. B. (1978), A critical look at long-term sun-weather relationships, *Rev. Geophys.*, *16*, 400–420.

Scafetta, N., and B. J. West (2005), Estimated solar contribution to the global surface warming using the ACRIM TSI satellite composite, *Geophys. Res. Lett.*, *32*, L18713, doi:10.1029/2005GL023849.

Schneider, T., and I. M. Held (2001), Discriminants of twentieth-century changes in Earth surface temperatures, *J. Clim.*, *14*, 249–254.

Stevens, M. J., and G. R. North (1996), Detection of the climate response to the solar cycle, *J. Atmos. Sci.*, *53*, 2594–2608.

van Loon, H., et al. (2004), A decadal solar effect in the tropics in July–August, *J. Atmos. Sol. Terr. Phys.*, *66*, 1767–1778.

van Loon, H., G. A. Meehl, and D. J. Shea (2007), Coupled air-sea response to solar forcing in the Pacific region during northern winter, *J. Geophys. Res.*, *112*, D02108, doi:10.1029/2006JD007378.

White, W. B., J. Lean, D. R. Cayan, and M. D. Dettinger (1997), Response of global upper ocean temperature to changing solar irradiance, *J. Geophys. Res.*, *102*, 3255–3266.

Wilson, R. C., et al. (1981), Observation of solar irradiance variability, *Science*, *211*, 700–702.

C. D. Camp and K. K. Tung, Department of Applied Mathematics, University of Washington, Seattle, WA 98195, USA. (tung@amath.washington.edu)